Stability control of a double inverted pendulum using a decoupled backstepping slidingmode strategy

Danh-Huy Nguyen[1], Van-Truong Nguyen[1], Trung-Hieu Luong[1], Xuan-Truong Vu[1] and Thi-Van-Anh Nguyen[1*]

[1] *School of Electrical and Electronic Engineering, Hanoi University of Science and Technology, Hanoi 100000, Vietnam*
[*] *Corresponding author E-mail: anh.nguyenthivan1@hust.edu.vn*
DOI: https://doi.org/10.64032/mca.v29i4.326

Abstract

The double inverted pendulum on a cart (DIPC) is a classical benchmark in nonlinear control due to its high instability, underactuated structure, and complex dynamic behavior. Traditional control approaches, such as Linear Quadratic Regulators (LQR) or conventional Sliding Mode Control (SMC), often face limitations in robustness and dynamic decoupling when applied to such systems. In response to these challenges, this study presents a Decoupled Backstepping Sliding Mode Control (DB-SMC) strategy that integrates the systematic design framework of backstepping with the robustness properties of sliding mode control. By introducing intermediate virtual control surfaces, the DB-SMC method effectively decouples the dynamics of the cart and the two pendulums, simplifying controller design and improving system stability. The control law is derived using Lyapunov stability theory to ensure convergence and robustness in the presence of uncertainties. Simulation results demonstrate that the proposed method achieves fast convergence, reduced overshoot, and strong disturbance rejection compared to traditional methods. The effectiveness of the DB-SMC controller highlights its potential for broader applications in nonlinear and underactuated systems.

Keywords: *Double Inverted Pendulum; Nonlinear Control; Backstepping; Sliding Mode Control*

1. Introduction

Inverted pendulum systems have long served as a fundamental benchmark for evaluating advanced control algorithms due to their nonlinear, underactuated, and inherently unstable nature [1, 2]. Among these, the double inverted pendulum on a cart (DIPC) represents a particularly challenging configuration, as it involves controlling two interconnected pendulum arms mounted atop a mobile cart [3, 4, 5, 6]. This structure introduces strong coupling between subsystems and increases the control complexity, making it an ideal testbed for validating robust and intelligent control strategies.

The practical relevance of the DIPC model extends beyond academic curiosity. It serves as a simplified abstraction of complex engineering systems such as walking robots [7], crane systems [8, 9, 10], satellite attitude control [11], and multi-link robotic manipulators [12]. As such, developing reliable control schemes for the DIPC not only advances theoretical understanding but also contributes to the broader field of modern automation and robotics.

Traditional linear control techniques such as Proportional-Integral-Derivative (PID) controllers [13, 14] and Linear Quadratic Regulators (LQR) [15, 16, 17] offer relatively straightforward implementation. However, their performance significantly deteriorates in the presence of system nonlinearities, parameter variations, and external disturbances. To overcome these drawbacks, nonlinear control approaches have been extensively investigated, including energy-based methods, feedback linearization, and fuzzy logic controllers.

Among the nonlinear strategies, Sliding Mode Control (SMC) has gained popularity for its inherent robustness against model uncertainties and external perturbations [18, 19, 20, 21]. Nevertheless, classical SMC is often associated with chattering which may lead to undesirable vibrations or even actuator damage. Additionally, SMC does not inherently offer a systematic framework for handling multi-state or hierarchical systems like the DIPC.

In contrast, backstepping control provides a recursive design methodology tailored for strict-feedback nonlinear systems [22, 23]. It facilitates the construction of stabilizing control laws based on Lyapunov functions at each step. However, pure backstepping approaches may lack the robustness required in real-world applications, particularly when dealing with unmodeled dynamics or abrupt external forces.

To harness the strengths of both techniques, this paper proposes a hybrid control framework known as Decoupled Backstepping Sliding Mode Control (DB-SMC). This approach merges the robustness and disturbance rejection of SMC with the systematic design process of backstepping control. By introducing virtual control surfaces, the DB-SMC method decouples the system's dynamics and facilitates hierarchical control design. The control laws are developed to ensure asymptotic stability of all state variables, and the design is validated using Lyapunov stability analysis.

The effectiveness of the proposed DB-SMC controller is evaluated through numerical simulations. The results demonstrate improved stabilization performance, fast convergence, and strong robustness under a variety of initial conditions and system uncertainties. These findings highlight the suitability of the proposed method for practical implementation in complex underactuated systems.

The remainder of this paper is organized as follows.

Received on 05 April 2025; Revised on 25 April 2025; Accepted on 23 May 2025.

Section 2 presents the mathematical modeling of the double inverted pendulum system. Section 3 describes the design of the DB-SMC controller in detail. Section 4 provides simulation results. Finally, Section 5 concludes the paper and suggests future research directions.

2. Mathematical modeling of the double inverted pendulum system

The double inverted pendulum on a cart is an inherently unstable and highly nonlinear system, often utilized to test advanced control strategies. To simplify the modeling procedure, minor factors such as air resistance and frictional forces are neglected, leading to an idealized mechanical system composed of a cart and two inverted pendulums as depicted in Figure 1.

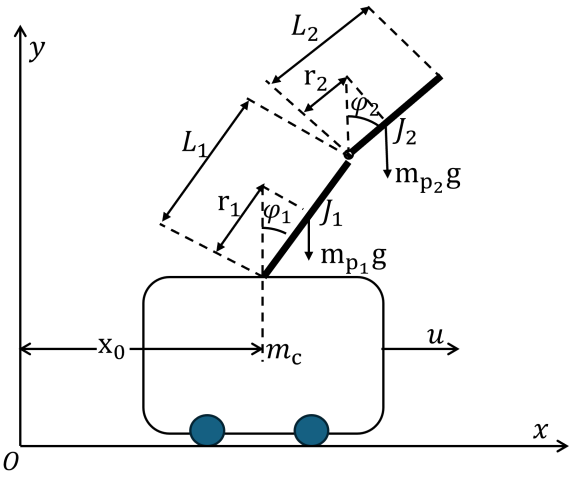

Hình 1: The double inverted pendulum on a cart.

The equations of motion for the double inverted pendulum are derived using Lagrange's method, expressed as:

$$\frac{d}{dt}\left(\frac{\partial L}{\partial \dot{\varphi}}\right) - \frac{\partial L}{\partial \varphi} = Q \tag{1}$$

where L is the Lagrangian defined by the difference between kinetic energy T and potential energy P:

$$L = T - P \tag{2}$$

and Q represents generalized external forces and torques acting on the system.

The generalized coordinates for describing the double inverted pendulum system are represented as:

$$\varphi = \begin{bmatrix} x_0 & \varphi_1 & \varphi_2 \end{bmatrix}^T \tag{3}$$

where x_0 denotes the horizontal displacement of the cart, and φ_1, φ_2 represent the angular displacements of the first and second pendulums, respectively.

The positions and velocities of both pendulums are functions of the cart position x_0, pendulum lengths L_1, L_2, and their respective angular positions φ_1, φ_2. Utilizing Lagrange's equations, the system's equations of motion can thus be derived and written explicitly as follows:

$$\frac{d}{dt}\left(\frac{\partial L}{\partial \dot{x}_0}\right) - \frac{\partial L}{\partial x_0} = u \tag{4}$$

$$\frac{d}{dt}\left(\frac{\partial L}{\partial \dot{\varphi}_1}\right) - \frac{\partial L}{\partial \varphi_1} = 0 \tag{5}$$

$$\frac{d}{dt}\left(\frac{\partial L}{\partial \dot{\varphi}_2}\right) - \frac{\partial L}{\partial \varphi_2} = 0 \tag{6}$$

The dynamic equations governing the motion of the system are formulated as follows:

$$\begin{aligned}
u &= (m_c + m_{p_1} + m_{p_2})\ddot{x}_0 + (m_{p_1} r_1 + m_{p_2} L_1)\cos(\varphi_1)\ddot{\varphi}_1 \\
&\quad + m_{p_2} r_2 \sin(\varphi_2)\ddot{\varphi}_2 \\
&\quad - (m_{p_1} r_1 + m_{p_2} L_1)\sin(\varphi_1)\dot{\varphi}_1^2 - m_{p_2} r_2 \sin(\varphi_2)\dot{\varphi}_2^2 \\
0 &= (m_{p_1} r_1 + m_{p_2} L_1)\cos(\varphi_1)\ddot{x}_0 + (m_{p_1} r_1^2 + m_{p_2} L_1^2 + J_1)\ddot{\varphi}_1 \\
&\quad + m_{p_2} L_1 r_2 \cos(\varphi_1 - \varphi_2)\ddot{\varphi}_2 + m_{p_2} L_1 r_2 \sin(\varphi_1 - \varphi_2)\dot{\varphi}_2^2 \\
&\quad - (m_{p_1} r_1 + m_{p_2} L_1) g \sin(\varphi_1) \\
0 &= m_{p_2} r_2 \cos(\varphi_2)\ddot{x}_0 + m_{p_2} L_1 r_2 \cos(\varphi_1 - \varphi_2)\ddot{\varphi}_1 \\
&\quad + (m_{p_2} r_2^2 + J_2)\ddot{\varphi}_2 - m_{p_2} L_1 r_2 \sin(\varphi_1 - \varphi_2)\dot{\varphi}_1^2 \\
&\quad - m_{p_2} r_2 g \sin(\varphi_2)
\end{aligned}$$

These equations can also be represented in matrix form as:

$$D(\varphi)\ddot{\varphi} + C(\varphi, \dot{\varphi})\dot{\varphi} + G(\varphi) = Hu \tag{7}$$

where:

$$D(\varphi) = \begin{pmatrix} \rho_1 & \rho_2 \cos(\varphi_1) & \rho_3 \cos(\varphi_2) \\ \rho_2 \cos(\varphi_1) & \rho_4 & \rho_5 \cos(\varphi_1 - \varphi_2) \\ \rho_3 \cos(\varphi_2) & \rho_5 \cos(\varphi_1 - \varphi_2) & \rho_6 \end{pmatrix}$$

$$C(\varphi, \dot{\varphi}) = \begin{pmatrix} 0 & -\rho_2 \sin(\varphi_1)\dot{\varphi}_1 & -\rho_3 \sin(\varphi_2)\dot{\varphi}_2 \\ 0 & 0 & \rho_5 \sin(\varphi_1 - \varphi_2)\dot{\varphi}_2 \\ 0 & -\rho_5 \sin(\varphi_1 - \varphi_2)\dot{\varphi}_1 & 0 \end{pmatrix}$$

$$G(\varphi) = \begin{pmatrix} 0 \\ -\rho_2 g \sin(\varphi_1) \\ -\rho_3 g \sin(\varphi_2) \end{pmatrix}; H = \begin{bmatrix} 1 & 0 & 0 \end{bmatrix}^T.$$

Here, the constants p_1 through p_6 are defined as follows:

$$\rho_1 = m_c + m_{p_1} + m_{p_2}, \quad \rho_2 = m_{p_1} r_1 + m_{p_2} L_1, \quad \rho_3 = m_{p_2} r_2$$

$$\rho_4 = m_{p_1} r_1^2 + m_{p_2} L_1^2 + J_1, \quad \rho_5 = m_{p_2} L_1 r_2, \quad \rho_6 = m_{p_2} r_2^2 + J_2$$

These constants correspond to combinations of the cart and pendulum masses, geometric dimensions, and moments of inertia, and are used to simplify the compact matrix representation of the system dynamics.

The system's acceleration can be expressed as:

$$\ddot{\varphi} = -D^{-1}(\varphi)C(\varphi, \dot{\varphi})\dot{\varphi} - D^{-1}(\varphi)G(\varphi) + D^{-1}(\varphi)Hu \tag{8}$$

To facilitate control design, the nonlinear dynamic behavior of the system can alternatively be represented in a state-space form as:

$$\begin{aligned}
\dot{x}_1(t) &= x_2(t) \\
\dot{x}_2(t) &= f_0(x) + g_0(x)u(t) \\
\dot{x}_3(t) &= x_4(t) \\
\dot{x}_4(t) &= f_1(x) + g_1(x)u(t) \\
\dot{x}_5(t) &= x_6(t) \\
\dot{x}_6(t) &= f_2(x) + g_2(x)u(t)
\end{aligned} \tag{9}$$

where $f_i(x)$ and $g_i(x)$ (for $i = 0, 1, 2$) are nonlinear functions representing the system dynamics, $x = [x_1, x_2, x_3, x_4, x_5, x_6]^T$ is the state vector, and $u(t)$ is the control input.

3. Control design approach

To provide a clearer understanding of the proposed system and control architecture, Figure 2 presents a structural diagram of the double inverted pendulum on a cart. This diagram illustrates the dynamic interaction among the system states and highlights how the controller intervenes to maintain balance and ensure stability.

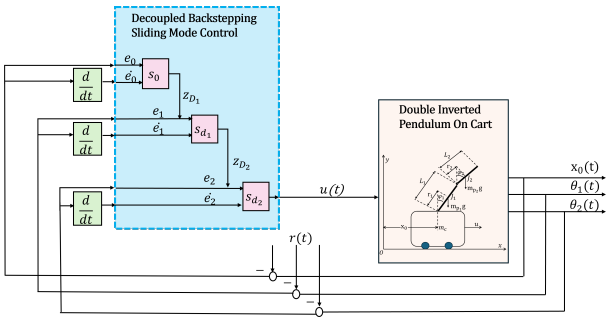

Hình 2: Overall structure of the DB-SMC-controlled double inverted pendulum system.

Controlling a double inverted pendulum on a cart is a challenging task due to its highly nonlinear nature, underactuated structure, and inherent instability. Classical control strategies, such as Linear Quadratic Regulator (LQR) or traditional Sliding Mode Control (SMC), often exhibit limitations when it comes to dynamic decoupling and robustness against model uncertainties or external disturbances.

To overcome these limitations, this work adopts the Decoupled Backstepping Sliding Mode Control (DB-SMC) approach. This hybrid control strategy merges the systematic design benefits of backstepping with the strong robustness properties of sliding mode control. DB-SMC enables effective decoupling of the system's nonlinear dynamics, facilitating the design of individual controllers for each subsystem while ensuring overall system stability and disturbance rejection. As a result, this method provides enhanced control performance for the complex dynamics of the double inverted pendulum system.

The tracking error associated with the cart displacement is denoted by e_0, e_1 for the angle of pole 1 and e_1 for the angle of pole 2 as

$$\begin{aligned} e_0(t) &= x_1(t) - y_{d_0} \\ e_1(t) &= x_3(t) - y_{d_1} \\ e_2(t) &= x_5(t) - y_{d_2} \end{aligned} \tag{10}$$

Taking the time derivatives of these errors yields:

$$\begin{aligned} \dot{e}_0(t) &= \dot{x}_1(t) - \dot{y}_{d_0} = x_2(t) - \dot{y}_{d_0} \\ \dot{e}_1(t) &= \dot{x}_3(t) - \dot{y}_{d_1} = x_4(t) - \dot{y}_{d_1} \\ \dot{e}_2(t) &= \dot{x}_5(t) - \dot{y}_{d_2} = x_6(t) - \dot{y}_{d_2} \end{aligned} \tag{11}$$

Considering a Lyapunov function candidate

$$V_{D_1}(e) = \frac{1}{2} e_2^2(t) \tag{12}$$

and differentiating it yields:

$$\dot{V}_{D_1}(e) = e_2(t)\dot{e}_2(t) = e_2(t)(x_6(t) - \dot{y}_{d_2}) \tag{13}$$

To proceed with the DBSMC framework, three sliding surfaces are introduced:

$$\begin{aligned} s_0(t) &= c_0 e_0(t) + \dot{e}_0(t) \\ s_1(t) &= c_1 e_1(t) + \dot{e}_1(t) \\ s_2(t) &= c_2 e_2(t) + \dot{e}_2(t) \end{aligned} \tag{14}$$

where c_0 , c_1 and c_2 are real positive constants.

Due to $x_6(t) - \dot{y}_{d_2} = s_2 - c_2 e_2(t)$ so:

$$\dot{V}_{D_1}(e) = e_2(t)s_2(t) - c_2 e_2^2 \tag{15}$$

$\dot{V}_{D_1}(e) = -c_2 e_2^2(t)$ is negative definite if and only if $s_2(t) = 0$. Therefore, to ensure the stability of the DBSMC system, an extended Lyapunov function is selected for the next design step, defined as:

$$V_{D_2}(e) = V_{D_1}(e) + \frac{1}{2} s_2^2(t) \tag{16}$$

Taking the time derivative of Eq.(15) and substituting Eq.(8) yields:

$$\begin{aligned} \dot{V}_{D_2}(e) &= \dot{V}_{D_1}(e) + s_2(t)\dot{s}_2(t) \\ &= e_2(t)s_2(t) - c_2 e_2^2(t) \\ &\quad + s_2(t)(f_2(x) + g_2(x)u_D(t)) \\ &\quad + s_2(t)(c_2\dot{e}_2(t) - \ddot{y}_{d_2}). \end{aligned} \tag{17}$$

To guarantee that $\dot{V}_{D_2}(e)$ is negative definite, the decoupled backstepping control law is selected as follows:

$$\begin{aligned} u_{D_{\text{eq}}}(t) &= \frac{1}{g_2(x)}\big(-f_2(x) - e_2(t) - c_2\dot{e}_2(t)\big) \\ &\quad + \frac{1}{g_2(x)}\big(\ddot{y}_{d_2} - c_3 s_2(t)\big). \end{aligned} \tag{18}$$

where c_3 is a positive real constant. To guarantee system stability, the switching control law can be formulated as follows:

$$u_{D_{\text{sw}}}(t) = -\frac{1}{g_2(x)} C\,\text{sign}(s_2(t)). \tag{19}$$

in which C is real positive constant.
The control law $u_D(t)$ is defined by combining the control laws from Eq. (17) and Eq. (18)

$$u_D(t) = u_{D_{\text{eq}}}(t) + u_{D_{\text{sw}}}(t). \tag{20}$$

Substituting Eq. (19) into Eq. (16) results in:

$$\dot{V}_{D_2}(e) = -c_2 e_2^2(t) - c_3 s_2^2(t) - C|s_2(t)| \leq 0.$$

Thus, the Lyapunov stability condition is satisfied.

To design a decoupled controller, a virtual sliding surface s_{d1} can be considered as follows:

$$s_{d_1}(t) = c_1(e_1(t) - z_{D_1}) + \dot{e}_1(t) \tag{21}$$

where z_{D_1} is an intermediate value derived from s_0 and is defined as follows:

$$z_{D_1}(t) = \text{sat}\left(\frac{s_0(t)}{\Delta_{D_{z_1}}}\right) z_{Du_1}, \quad 0 < z_{Du_1} < 1 \tag{22}$$

where z_{Du_1} represents the upper bound of $z_{D_1}(t)$, and $\Delta_{D_{z_1}}$ is a constant that defines the boundary layer width. The parameter $\Delta_{D_{z_1}}$ serves to scale $s_0(t)$ into an appropriate range for influencing $e_1(t)$.

An additional decoupled controller is designed to describe the effect of the selected virtual sliding surface s_{d_1} on the sliding surface s_2.

$$s_{d_2}(t) = c_2(e_2(t) - z_{D_2}) + \dot{e}_2(t) \tag{23}$$

where z_{D_2} is an intermediate value transferred from s_{d_1} and is defined as follows:

$$z_{D_2}(t) = \text{sat}\left(\frac{s_{d_1}(t)}{\Delta_{D_{z_2}}}\right) z_{Du_2}, \quad 0 < z_{Du_2} < 1 \tag{24}$$

where z_{Du_2} denotes the upper bound of $z_{D_2}(t)$, and $\Delta_{D_{z_2}}$ is a constant that defines the boundary layer width. The parameter $\Delta_{D_{z_2}}$ is used to scale $s_{d_1}(t)$ into a suitable range for controlling $e_2(t)$. where Φ_s is the boundary layer of s_2 to smooth, Φ_s transfers s_2 to the proper range of x_1, and the definition of sat$(\cdot)$ function is the same as (10). Notice that z is a decaying oscillation signal because z_1 is a factor less than one.

As s_{d_1} decreases, z_{D_1} decreases, too. When $s_{d_1} \to 0$, then $z_{D_1} \to 0$ in (21), when $s_{d_1} \to 0$, then $z_{D_2} \to 0$, then $s_{d_2} \to 0$ and the control objective can be achieved.

Finally, we obtain the control law for the DBSMC method.

$$\begin{aligned} u_D(t) = & \frac{1}{g_2(x)}(-f_2(x) - e_2(t) - c_2\dot{e}_2(t)) \\ & + \frac{1}{g_2(x)}(\ddot{y}_{d_2} - c_3 s_{d_2}(t)) \\ & - \frac{1}{g_2(x)} C\,\text{sign}(s_{d_2}(t)). \end{aligned} \tag{25}$$

4. Simulation results

The controller parameters used in the simulation are selected to ensure system stability and effective performance under the DB-SMC strategy. Specifically, the sliding surface coefficients are set as $c_0 = 0.2$, $c_1 = 1$, $c_2 = 6.5$, and $c_3 = 1$. The gain of the switching control component is chosen as $C = 6$, while the saturation boundary parameter is defined as $\Delta = 5$. In the design of the virtual control surfaces, the boundary layer widths are set to $\Delta D_{z_1} = \Delta D_{z_2} = 5$, and the upper limits for the saturation functions are specified as $z_{Du_1} = z_{Du_2} = 0.92$. These parameter values are tuned to balance control performance, robustness, and smoothness of the system response.

Table 1 lists the physical parameters of the double inverted pendulum on cart (DIPC) system used in the simulations.

Bảng 1: Parameters of DIPC.

Symbol	Unit	Description	Value
m_c	kg	Cart mass	0.8
m_{p_1}	kg	Mass of the first pendulum	0.5
m_{p_2}	kg	Mass of the second pendulum	0.3
L_1	m	Length of the first pendulum	0.3
L_2	m	Length of the second pendulum	0.2
J_1	$\text{kg} \cdot m^2$	Inertia of the first pendulum	0.006
J_2	$\text{kg} \cdot m^2$	Inertia of the second pendulum	0.006
g	m/s^2	Gravitational acceleration	9.8

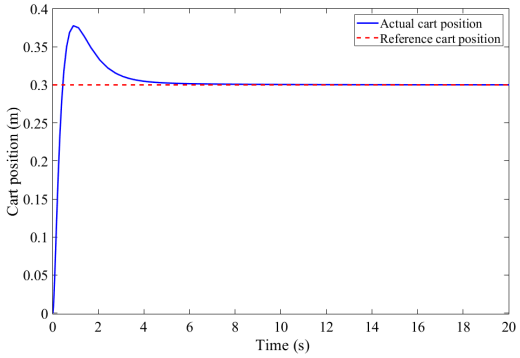

(a) Cart Position

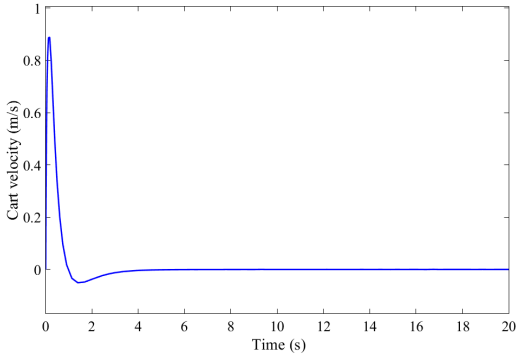

(b) Cart Velocity

Hình 3: Position and velocity of the cart.

The simulation is conducted using the DIPC system parameters listed in Table 1, with the initial conditions set as $x_0 = 0$ m, $\varphi_1 = \frac{\pi}{12}$ rad, and $\varphi_2 = 0.1$ rad.

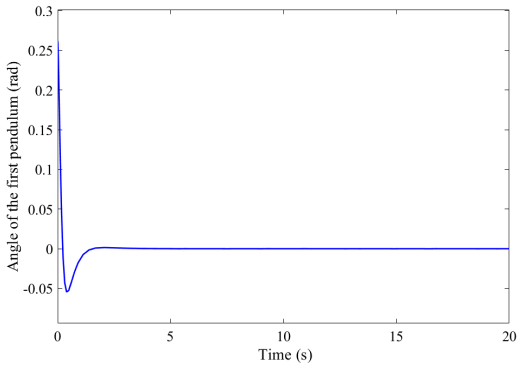

(a) Angle of the first pendulum

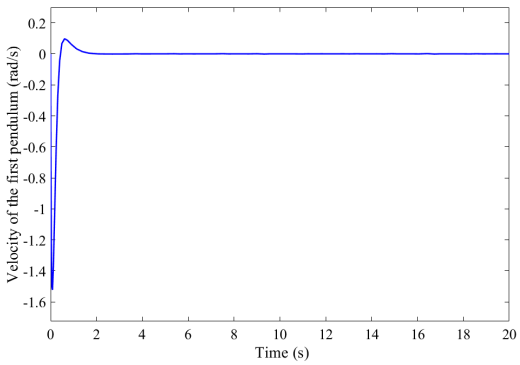

(b) Velocity of the first pendulum

Hình 4: Angle and velocity of the first pendulum.

Figure 3 illustrates the cart's position and velocity responses over time. As shown in Figure 3(a), the cart position initially

experiences a noticeable overshoot before gradually converging to the desired reference position. Figure 3(b) shows that the cart velocity exhibits a rapid initial decrease, followed by minor oscillations, and stabilizes near zero after approximately 3 seconds. These results demonstrate that the controller successfully stabilizes the cart, although further tuning could help minimize the overshoot and improve convergence speed.

Figure 4 presents the dynamic response of the first pendulum in terms of angular displacement and angular velocity. As shown in Figure 4(a), the angle of the first pendulum exhibits a small overshoot before gradually stabilizing around the equilibrium position within approximately 3 seconds. In Figure 4(b), the corresponding angular velocity initially fluctuates but reaches a steady-state condition around the 2-second mark, indicating effective damping and convergence.

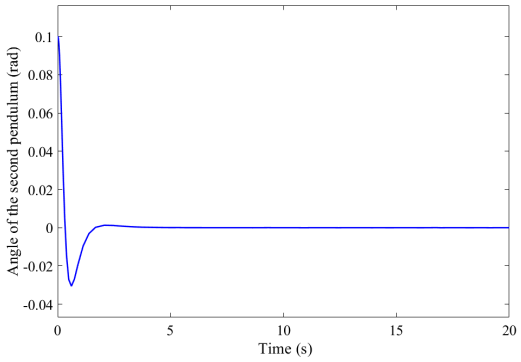

(a) Angle of the second pendulum

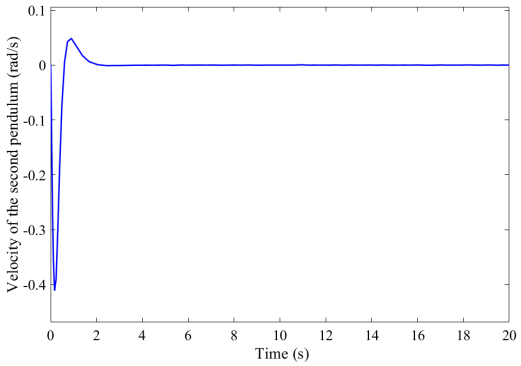

(b) Velocity of the second pendulum

Hình 5: Angle and velocity of the second pendulum.

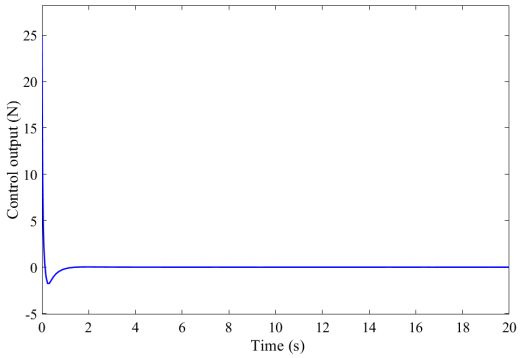

Hình 6: Control Signal.

Figure 5 illustrates the response of the second pendulum. In Figure 5(a), the angle stabilizes after a short transient phase, settling to its steady-state value around 4 seconds. The angular velocity shown in Figure 5(b) demonstrates rapid convergence with minor oscillations, achieving stability approximately 2.5 seconds after the control is applied. These results confirm the controller's ability to regulate the pendulum dynamics with minimal steady-state error and acceptable transient behavior. Figure 6 illustrates the control input applied to the system over time. At the start, the control signal exhibits a sharp peak reaching approximately 25 N, reflecting the controller's rapid response to the system's initial imbalance. Following this initial surge, the control effort quickly decreases and settles into a nearly constant value with minimal oscillations. This behavior highlights the effectiveness of the proposed DB-SMC controller in achieving fast corrective action while maintaining system stability and control efficiency during steady-state operation.

5. Robustness analysis

5.1 Effect ofparametervariations

The Figure 7 illustrates the position of the cart over time with changes in the mass parameters. The position of the cart stabilizes quickly within 2-3 seconds for all mass configurations, indicating that the system's response is fast and efficient. Despite changes in the masses of the cart and pendulums (m_c, m_{p_1}, m_{p_2}) the stable position remains largely unaffected, showing that the system has strong robustness against parameter variations. The convergence time is almost unaffected across different mass configurations, further highlighting the effectiveness and stability of the control system.Although there are slight differences in the transient process, these oscillations decrease quickly, and the system remains stable.

The angle of the first pendulum in Figure 8 stabilizes quickly across all mass configurations, with minimal differences in the final stable position. The change in mass (m_c, m_{p_1}, m_{p_2}) has little impact on the stable angle, which converges near 0 rad. The system's convergence time is around 2-3 seconds. The transient response in Figure 8 shows initial oscillations before the system reaches the stable state.

The angle of the second pendulum in Figure 9 stabilizes quickly within about 2-3 seconds, with minimal difference in the final position across mass configurations. The mass changes (m_c, m_{p_1}, m_{p_2}) have little effect on the stable angle.

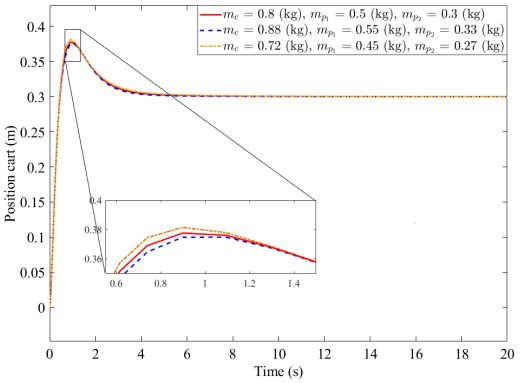

Hình 7: Position of cart when change parameters.

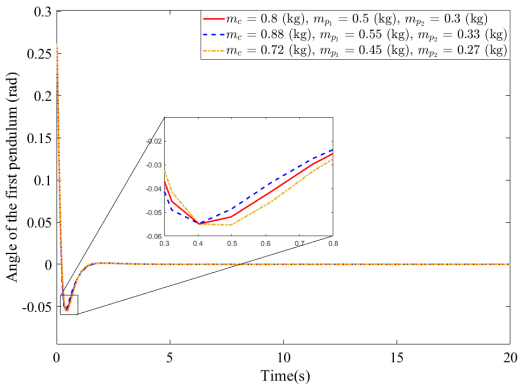

Hình 8: Angle of the first pendulum when change parameters.

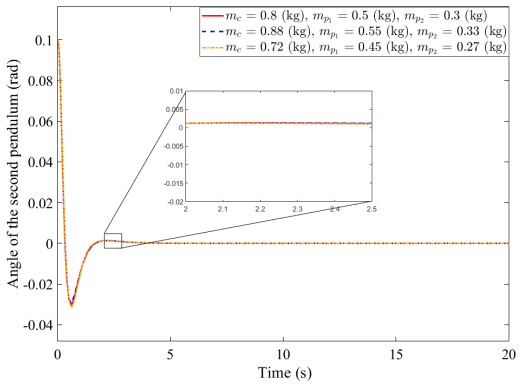

Hình 9: Angle of the second pendulum when change parameters.

5.2 Effect ofinitial conditions

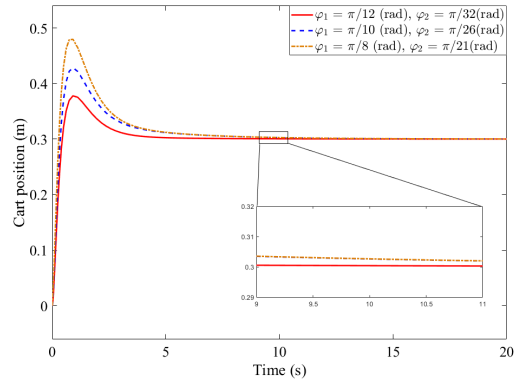

Hình 10: Cart position with varying initial pendulum angles.

The inverted pendulum system on the cart using the Decoupled Backstepping Sliding Mode Control controller in Figure 10 shows relatively significant oscillations during the transient phase, especially with larger changes in the tilt angle ($\varphi_1 = \pi/8$ rad). When the initial angles φ_1 and φ_2 are larger, the convergence time of the cart is longer, around 9-10 seconds. This convergence time indicates that the controller effectively adjusts the system to bring it to a stable state. However, the larger oscillations in cases with higher φ_1 demonstrate the system's sensitivity to changes in input conditions.

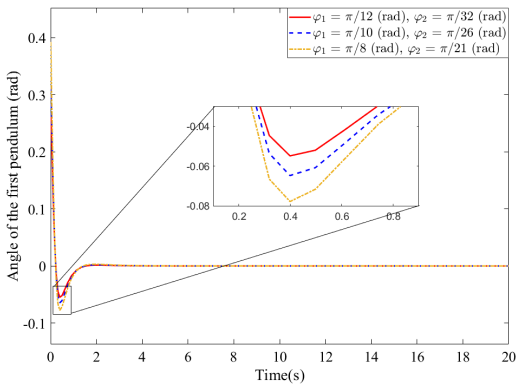

Hình 11: Angle of first pendulum with varying initial pendulum angles.

The Figure 11 shows the angle of the first pendulum when the initial values are changed. The system exhibits moderate oscillations during the transient phase, but it stabilizes quickly within approximately 3–4 seconds. The convergence time for all cases is nearly the same, indicating that the Decoupled Backstepping Sliding Mode Control (DBSMC) controller is effective in stabilizing the system. The differences between the curves are mainly due to changes in the initial tilt angle (φ_1), but they do not significantly affect the convergence time. The controller successfully drives the system to convergence despite changes in the input conditions.

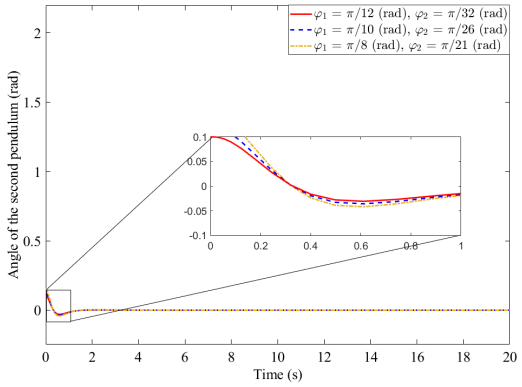

Hình 12: Angle of second pendulum with varying initial pendulum angles.

The Figure 12 shows the angle of the second pendulum when the initial values are varied. The angle of the second pendulum exhibits relatively small oscillations during the transient phase, with the system stabilizing quickly within about 2 seconds. The convergence time is consistent across all initial conditions, reaching a stable value near zero. The oscillations are minimal, even with varying initial angles ($\varphi_1 = \pi/8$ rad and $\varphi_2 = 0.15$ rad). Overall, the Decoupled Backstepping Sliding Mode Control (DBSMC) efficiently stabilizes the system with very little oscillation, demonstrating strong robustness to initial condition variations.

5.3 Robustness against Actuator Disturbance

The Figure 13 shows the position of the cart when the control signal is affected by disturbance. The system experiences significant oscillations in the initial phase but then stabilizes at a position close to 0.3 m. However, the disturbance

causes small oscillations around the stable position throughout the process, indicating that the system is still affected by the disturbance even after stabilizing.

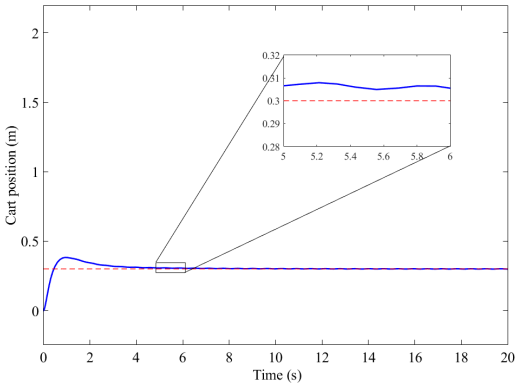

Hình 13: Effect of actuator disturbance on cart position.

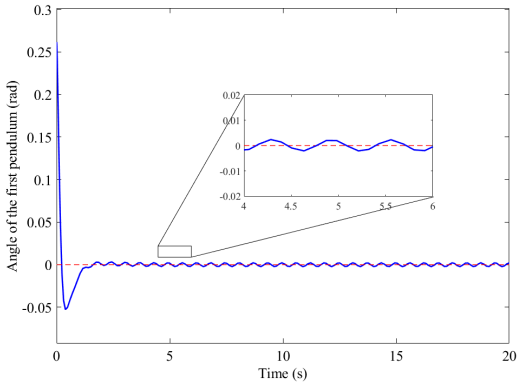

Hình 14: Effect of actuator disturbance on angle of the first pendulum.

The Figure 14 shows the angle of the first pendulum when the control signal is affected by disturbance. The system experiences significant initial oscillations, then stabilizes around 0 rad after 2 seconds, with small oscillations continuing around the stable value. The disturbance causes high-frequency oscillations, but the system eventually stabilizes.

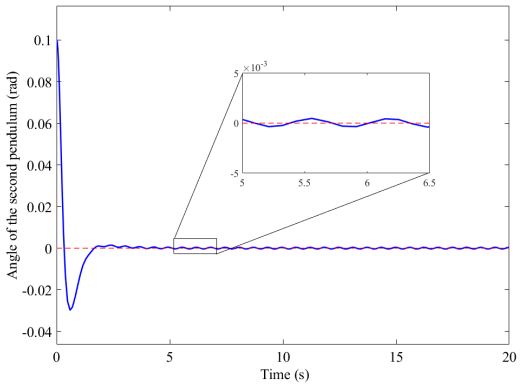

Hình 15: Effect of actuator disturbance on angle of the second pendulum.

The Figure 15 illustrates the angle of the second pendulum when the control signal is influenced by disturbance. Similar to the first pendulum, the system stabilizes around 0 rad after a short transient period.

6. Comparative analysis

To ensure a fair and comprehensive evaluation, the comparative analysis of the Decoupled Backstepping Sliding Mode Control (DBSMC) and the Linear Quadratic Regulator (LQR) methods for the double inverted pendulum on a cart is conducted under identical initial conditions and parameter settings. Both methods are tested with the same starting states for the cart position (x_0) and pendulum angles (φ_1 and φ_2), as well as consistent system parameters, including mass, length, and damping coefficients. This controlled setup allows for a direct assessment of their performance using two key metrics: Normalized Mean Absolute Error (NMAE) and Normalized Root Mean Square Error (NRMSE), which reflect the accuracy and stability of each control strategy.

Normalized Mean Absolute Error (NMAE): Measures the average absolute error, normalized by the data range.

$$\text{NMAE} = \frac{1}{n}\sum_{i=1}^{n}\frac{|y_i - \hat{y}_i|}{y_{\max} - y_{\min}} \tag{26}$$

Normalized Root Mean Square Error (NRMSE): Quantifies the root mean square error, normalized by the data range.

$$\text{NRMSE} = \frac{\sqrt{\frac{1}{n}\sum_{i=1}^{n}(y_i - \hat{y}_i)^2}}{y_{\max} - y_{\min}} \tag{27}$$

- y_i: Actual value at the i-th data point
- $\hat{y}_i$: Predicted value at the i-th data point
- $y_{\max}$: Maximum value among all actual values
- $y_{\min}$: Minimum value among all actual values
- n: Total number of data points.

Bảng 2: Comparison of LQR and DBSMC methods.

Parameter	Method	NMAE	NRMSE
x_0	LQR	0.126060	0.315009
	DBSMC	0.074983	0.218164
φ_1	LQR	0.074493	0.225001
	DBSMC	0.062164	0.209502
φ_2	LQR	0.082331	0.232393
	DBSMC	0.067422	0.210998

The results are summarized in Table2. For the cart position (x_0), DBSMC achieves an NMAE of 0.074983 and an NRMSE of 0.218164, representing a 40.5% reduction in NMAE and a 30.8% reduction in NRMSE compared to LQR (NMAE: 0.12606, NRMSE: 0.315009). For the pendulum angles, DBSMC also demonstrates superior performance: for φ_1, NMAE is 0.062164 and NRMSE is 0.209502, while for φ_2, NMAE is 0.067422 and NRMSE is 0.210998, showing improvements of 24.5% and 18.1% in NMAE, and 10.8% and 9.2% in NRMSE over LQR (NMAE: 0.082331, NRMSE: 0.232393 for φ_2).

These results highlight the robustness and adaptability of DBSMC, particularly in maintaining stability under dynamic conditions. The significant error reductions suggest that DBSMC offers a more effective control strategy for the double inverted pendulum system. Future research should explore its computational efficiency and real-time performance to further validate these findings.

7. Conclusion

This paper presented a Decoupled Backstepping Sliding Mode Control (DB-SMC) strategy for stabilizing a highly nonlinear and underactuated double inverted pendulum on a cart (DIPC). The proposed control scheme effectively combines the robustness of sliding mode control with the systematic design approach of backstepping, while introducing virtual control surfaces to decouple the system dynamics.

Through Lyapunov-based stability analysis, the control law was shown to guarantee convergence and robustness in the presence of external disturbances and modeling uncertainties. Simulation results validated the performance of the controller, demonstrating its ability to stabilize the cart and both pendulums with fast response, minimal overshoot, and strong disturbance rejection.

The DB-SMC approach proves to be a promising solution for complex nonlinear systems, particularly those with multiple degrees of instability and coupled dynamics. Future work may explore the extension of this method to adaptive or observer-based variants, as well as its experimental validation on real-time embedded platforms.

Acknowledgment

This research is funded by Hanoi University of Science and Technology (HUST) under project number T2024-TD-015.

Tài liệu

[1] Nguyen, T. V. A., Dao, Q. T., Bui, N. T. (2024). Optimized fuzzy logic and sliding mode control for stability and disturbance rejection in rotary inverted pendulum. Scientific Reports, 14(1), 31116.

[2] Dong, B. T., Nguyen, T. V. A. (2024). Simplified LMI Conditions for Takagi-Sugeno Fuzzy Observer Design with Unmeasured Premise Variables. International Journal of Fuzzy Systems, 1-12.

[3] Lee, T., Ju, D., Lee, Y. S. (2025). Transition Control of a Double-Inverted Pendulum System Using Sim2Real Reinforcement Learning. Machines, 13(3), 186.

[4] Maraslidis, G. S., Kottas, T. L., Tsipouras, M. G., Fragulis, G. F. (2022). Design of a fuzzy logic controller for the double pendulum inverted on a cart. Information, 13(8), 379.

[5] Zhu, D. X., Cui, N. (2024). Design of intelligent control for flexible linear double inverted pendulum based on particle swarm optimization algorithm. Systems Science Control Engineering, 12(1), 2332409.

[6] Phan, M. S., Do, T. C., Truong, V. Q., Nguyen, T. V. A. (2023). Comparative Analysis of SMC-LMI and LQR Controllers for Double Inverted Pendulum. Journal of Measurement, Control, and Automation, 4(3), 1-7.

[7] Biswal, P., Mohanty, P. K. (2021). Development of quadruped walking robots: A review. Ain Shams Engineering Journal, 12(2), 2017-2031.

[8] Tan, P., Liu, J., Sun, M., Chen, Z. (2025). Disturbance Compensation-Based Deep Reinforcement Learning Control Strategy for Underactuated Overhead Crane Systems: Design and Experiments. IEEE Transactions on Intelligent Transportation Systems.

[9] Nguyen, H. P., Bui, N. T. (2024). Tracking Control Based on Takagi-Sugeno Fuzzy Descriptor Model for Overhead Crane combined with Input Shaping. IEEE Access.

[10] Wu, Y., Wu, Q., Zhang, M., Guo, S., Zhai, M., Pang, R., Sun, N. (2025). A model predictive control method for 7-DoF tower cranes with distributed mass payloads and variable rope lengths. Mechanical Systems and Signal Processing, 229, 112513.

[11] Mezzi, W., Kiss, B. Magnetic torquers actuated satellite attitude control using linear parameter varying techniques. Journal of Dynamic Systems, Measurement, and Control, 1-32.

[12] Zuo, H., An, A., Yu, B., Niu, J., Xie, X. (2024, November). Combination Control Method of Multi-Link Flexible Manipulator. In 2024 China Automation Congress (CAC) (pp. 3753-3758). IEEE.

[13] Zeynivand, A., Moodi, H. (2022, March). Swing-up control of a double inverted pendulum by combination of Q-learning and PID algorithms. In 2022 8th International Conference on Control, Instrumentation and Automation (ICCIA) (pp. 1-5). IEEE.

[14] Li, H. R., Nie, Z. Y., Zhu, E. Z., He, W. X., Zheng, Y. M. (2021, December). Double loop DR-PID control of a rotary inverted pendulum. In 2021 IEEE International Conference on Networking, Sensing and Control (ICNSC) (Vol. 1, pp. 1-5). IEEE.

[15] Aslam, M. S., Bilal, H., Hayajneh, M. (2024). Lqr-based PID controller with variable load tuned with data-driven methods for double inverted pendulum. Soft Computing, 28(1), 325-338.

[16] Habib, M. K., Ayankoso, S. A. (2022, August). Hybrid control of a double linear inverted pendulum using LQR-fuzzy and LQR-PID controllers. In 2022 IEEE International Conference on Mechatronics and Automation (ICMA) (pp. 1784-1789). IEEE.

[17] Shala, E., Bajrami, X., Likaj, R., Pajaziti, A. (2023). Real Time Swinging Up and Stabilizing a Double Inverted Pendulum Using PID-LQR. Strojnícky casopis–Journal of Mechanical Engineering, 73(1), 159-168.

[18] Tong, T. L., Ho, M. T., Dao, H. H., Pham, V. K., Minh, D. D., Dao, Q. T. (2024). Tối Ưu Tham Số Bộ Điều Khiển Trượt cho Cẩu Tháp Sử Dụng Giải Thuật Tối Ưu Bầy Đàn. Journal of Measurement, Control, and Automation, 5(1), 30-38.

[19] Dinh, V. V., Mai, D. H., Duong, M. D., Dao, Q. T. (2024). Prescribed Performance Function Based Sliding Mode Control Of Opposing Pneumatic Artificial Muscles To Enhance Safety. Journal of Applied Science and Engineering, 27(2), 2117-2126.

[20] Shafeek, Y. A., Ali, H. I. (2024). Application of Particle Swarm Optimization to a Hybrid H/Sliding Mode Controller Design for the Triple Inverted Pendulum System. Algorithms, 17(10), 427.

[21] Cherrat, N., Boubertakh, H., Arioui, H., Fellag, R. (2024, November). Experimental Study of Swing-Up PD and Sliding Mode Control for Rotary Inverted Pendulum. In 2024 3rd International Conference on Advanced Electrical Engineering (ICAEE) (pp. 1-5). IEEE.

[22] Duong, M. D., Tran, T. T. (2024). DESIGNING OF DYNAMIC SURFACE CONTROL BASED ON BACKSTEPPING TECHNIQUE FOR SERIES ELASTIC ACTUATOR ROBOT. ASEAN Engineering Journal, 14(1), 85-92.

[23] Pham, V. H., Le, D. T., Nguyen, N. T., Dang, V. T., Nguyen-Thi, V. A., Nguyen, D. H., Nguyen, T. L. (2022, December). Backstepping sliding mode control design for active suspension systems in half-car model. In International Conference on Engineering Research and Applications (pp. 281-289). Cham: Springer International Publishing.